

OVERVIEW OF VERIFICATION AND VALIDATION EFFORTS FOR PDE-BASED LAMINAR-TURBULENT TRANSITION MODELS

James G. Coder[1]

[1]The Pennsylvania State University, University Park, PA 16801, United States

Abstract

Verification and validation of PDE-based laminar-turbulent transition models is an essential process, but one that is still the subject of ongoing discussion and community efforts. This paper describes some of those activities, including the AIAA CFD Transition Modeling and Prediction Workshop series. An overview of results and outcomes from the first workshop, held in 2021, is provided, but open questions still remain. There are also persisting challenges to model development as well as verification and validation efforts, and several of these are detailed. A second workshop will be held in 2027 to help address some of these in a concerted manner. The workshop is organized so that the low-speed, transonic, and hypersonic flight regimes can be addressed separately and independently under a Technology Focus Group paradigm. The specific test cases for each flight regime are also briefly described in this paper.

Keywords: CFD, RANS, Transition Modeling, Turbulence Modeling

1. Introduction

Laminar-turbulent transition modeling within RANS-based computational fluid dynamics solvers is an enabling technology for the design of ultra-efficient aircraft. The dominant forms of these models are based on the solution of partial-differential-equation transport equations, as these fit well within massively parallelized RANS solvers. Although models of this type have been available in the literature for over two decades, the technology is still somewhat nascent in its capabilities and application space. Numerous model forms have been proposed, including laminar-kinetic-energy models [1, 2], intermittency-based local-correlation models [3, 4], and amplification factor transport models [5, 6].

A pervasive challenge with transition models is the issue of verification and validation. Turbulence model verification, or lack thereof, was identified in the AIAA Drag Prediction Workshop series [7] as being a leading cause of code-to-code disagreement, which helped promote community-wide efforts to ensure that models are correctly implemented. Similar efforts have taken place for laminar-turbulent transition models, such as their inclusion on the NASA Turbulence Modeling Resource and promotion of standardized test cases [8], but the results have been less positive and not without challenges. One of the main issues is lack of consistency of model definitions across various codes. A contributor to this is that early publications of PDE-based models, such as in [9], did not include all necessary model correlations. This prompted many users to develop their own, often proprietary, correlations that persist in their code bases. With the added factor of the transition model needing to be coupled to a turbulence model, there is also a prevalence of various mix-and-match models, all with their own coupling strategies.

Even when developers and practitioners use as-published models, the numerical properties of existing models make verification challenging. For example, Venkatachari et al. [10] found that impractically fine mesh resolutions could be needed to attain asymptotic convergence. Aside from model

form, this is a consequence of the physics of natural transition, which requires convergence of the mean flow before the transition equations can converge. Thus, slight variations in the mean flow can cause major variations in the transition location. Another issue, identified by Gosin et al. [11], is that transition sensors can be easily contaminated by numerical error that does not damp well with mesh refinement or adaptation.

The objective of this paper is to provide a high-level overview of organized efforts related to model verification and validation, including prominent PDE model forms and persisting modeling challenges.

2. Summary of Prominent PDE Model Forms

After nearly two decades of PDE-based transition models being implemented in widely used commercial and government CFD codes, there are three general model forms that have emerged. All of these models qualify as "phenomenological" by the definition typically espoused by the author. [1] These are the Local Correlation Transition Models popularized by Menter (cf. [3, 4]), the Amplification Factor Transport paradigm developed by Coder [5], and the algebraic model of Cakmakçioglu, Bas, and Kaynak [12].

2.1 Local-Correlation Models

Local-correlation transition models (LCTMs) are single-point closure methods to determine whether the flow should transition to turbulence. A typical way of expressing their streamwise transition criterion is that they evaluate a local Reynolds number that is well-defined in laminar boundary layers, such as the vorticity Reynolds number, and compare it to a transitional value of the same Reynolds number. The heart of the model is in how it calculates the transitional Reynolds number, which may be a function of a local pressure gradient parameter and turbulence intensity. Experience with these models confirms strong performance in high-turbulence-intensity environments where bypass transition is dominant. They also provide reasonable predictions for external aerodynamic flows with lower turbulence intensity, but struggle to accurately capture the upstream movement of transition as lift increases [13].

The most prominent of these models are the Langtry-Menter $\gamma - Re_{\theta,t}$ [3] and the Menter-Smirnov γ [4] models. The Langtry-Menter model evaluates the transitional Reynolds number at the edge of the boundary layer and then uses a transported variable $\widetilde{Re_{\theta,t}}$ to diffuse it into the boundary layer. The Menter-Smirnov model evaluates the transition criterion inside the boundary layer with fully local quantities, allowing it to forgo the $\widetilde{Re_{\theta,t}}$ equation. Both models use a transported intermittency variable γ to carry the knowledge of transition downstream to activate the turbulence model. Menter et al. further evolved the model to use an algebraic intermittency model, thereby having a zero-equation transition model while still including sensitivity to turbulence intensity and pressure gradient [14].

The local-correlation modeling framework has also been extended by various groups to capture transition due to additional mechanisms, such as crossflow transition in three-dimensional flows (e.g. swept wings and bodies at incidence) [15, 16, 17] and second-mode transition at hypersonic conditions [18].

2.2 Amplification Factor Transport Models

The Amplification Factor Transport (AFT) modeling approach takes the idea of locally estimating a pressure-gradient parameter (or shape factor) and using it to drive a PDE that tracks the margin to transition. In this manner it is able to capture upstream history effects, offering additional capability over a local correlation model. The first AFT model, termed "AFT2014", was developed by Coder and Maughmer [5] and used a novel local shape factor along with the approximate envelop e^N model of Drela and Giles [19]. The AFT2014 shape factor relied on an isentropic outer-flow assumption, limiting its applicability to general cases. Later evolutions of the model (i.e., [20, 6]) switched to

[1] "Phenomenological" models track surrogate quantities associated with the transition process that are not directly measurable, whereas "physics-based" models attempt to directly predict measurable physical quantities.

the Menter-Smirnov pressure gradient parameter to allow more flexibility, whereas the original local shape factor has found recent success for transonic aircraft analysis [13, 21]. The AFT models may also be used in conjunction with local-correlation crossflow models [22].

Multiple researchers have extended the AFT model into the hypersonic regime, including Barraza et al. [23] and Liu et al. [18]. The underlying concept of the AFT model (that is, tracking a margin to transition) has also been employed to develop models that are not explicitly tied to an e^N method. Notable examples include the models of Ströer et al. [24] and Pascal et al. [25].

2.3 Bas-Cakmakçioglu Model

The algebraic model proposed by Cakmakçioglu, Bas, and Kaynak (often referred to as the Bas-Cakmakçioglu, or BC, model) [12] has garnered interest from the modeling community over the past several years. Although it does not have any direct accounting of pressure-gradient effects, the model formulation is very simple compared to LCTM and AFT models. As an algebraic model it does not increase the number of equations that need to be solved, furthering its appeal.

2.4 Other Model Types

The three modeling types listed above are not meant to be a comprehensive list, but rather a high-level assessment based on the author's experience. There are other modeling frameworks, such as the laminar-kinetic-energy models of Walters [1, 2] or the hypersonic laminar-eddy-viscosity model of Qiao et al. [26], that users may find suitable for their applications.

3. First AIAA CFD Transition Modeling and Prediction Workshop

The First AIAA CFD Transition Modeling and Prediction Workshop (CFDTMPW-1) was organized as an extension of the activities of the AIAA CFD Transition Modeling Discussion Group, sponsored by the Applied Aerodynamics Technical Committee. The discussion group focuses more on practical application of transition modeling with an emphasis on PDE-based models as a more care-free alternative to stability calculations. In this way it is distinct from interest groups that focus on the fundamental physics of boundary-layer transition; however, basic researchers are welcome to the discussion group to facilitate technology transfer. The workshop was originally scheduled to be in-person in summer 2020, but due to the COVID pandemic it was shifted to a virtual event held in January 2021. Four main objectives were identified:

- Assess the current state of the art in laminar-turbulent transition prediction in an industrial CFD environment
- Determine and document best practices for transitional flow simulations
- Verify transition/turbulence model implementations
- Encourage risk taking by participants and promote improvements to CFD prediction capabilities

Participant data were submitted by 18 teams, balanced across industry (4 teams), academia (7 teams), and government (7 teams). This categorization is based on the lead organization of the teams, though several teams were mixed across organization types. A particularly notable quality of the submitted data was that nearly every team used a different turbulence+transition model variant, which precluded meaningful code-to-code verification.

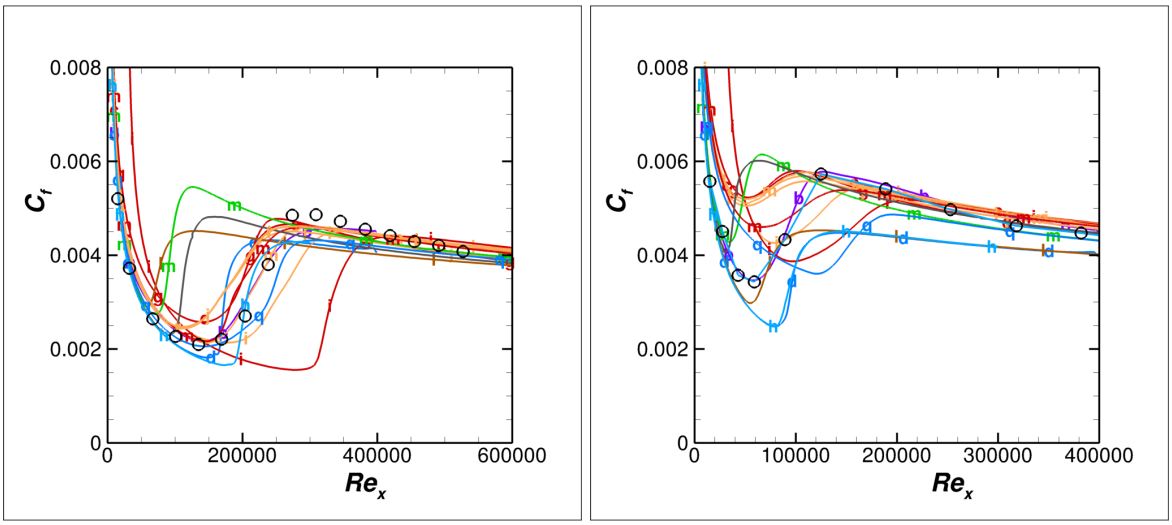
3.1 Test Cases and Representative Results

In preparation for the workshop, four distinct cases were identified to exercise the different predictive capabilities of common models. These test cases are 1) a zero-pressure-gradient (ZPG) flat plate at multiple turbulence intensities [27]; 2) the NLF(1)-0416 airfoil [28]; 3) a 6:1 prolate spheroid [29]; and 4) the natural-laminar-flow variant of the NASA/Boeing Common Research Model (CRM-NLF) [30]. Common families of structured/overset and unstructured grids were provided by the organizing committee, but participants were invited to generate their own grids following the provided meshing guidelines.

3.1.1 Case 1: ZPG Flat Plate

The first case, regarded as both a verification and validation case, was the T3A and T3B flat-plate cases. Both cases featured high free-stream turbulence intensity so that bypass transition is the transition mechanism. Tight coupling was observed between the grid dimensions and the turbulence intensity at the beginning of the plate, which drove the upstream location of the inlet for the committee-provided grids. Inlet conditions were specified based on the behavior of the SST turbulence model [31] (based on the prevalent use of Menter's transition models [3, 4]). Models based on the Spalart-Allmaras turbulence model [32] do not explicitly track the turbulence intensity, and they do not show any decay of the turbulence variables in quiescent free-stream flow.

Assessment of the participant results showed a wide spread in predicted transition location for both the T3A and T3B cases. The skin-friction predictions are shown in Fig. 1. While this spread could be attributed to different transition models, there was spread even between participants who used the same transition model but different turbulence models. Overall, the Menter models provided the most accurate predictions, due in part to these cases being part of their calibration database.



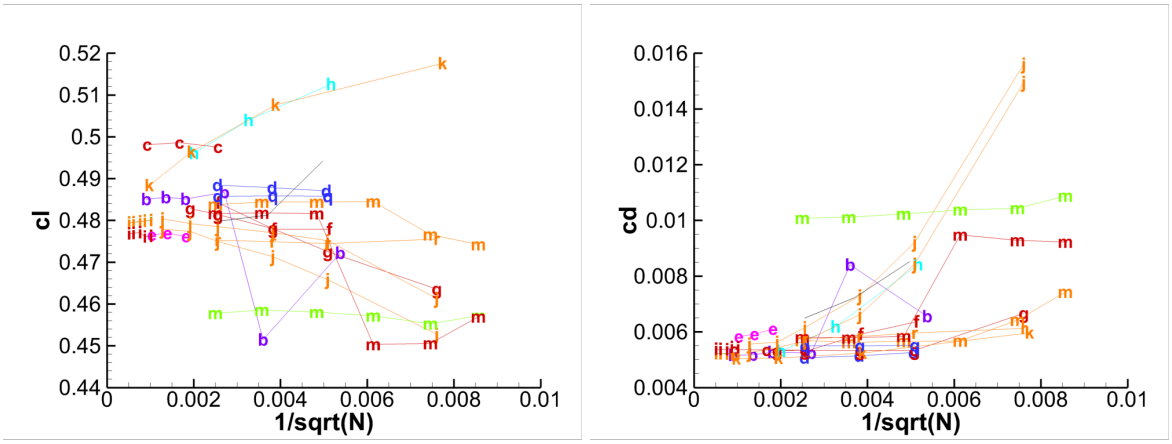
(a) T3A (b) T3B

Figure 1 – Comparison of predicted skin-friction distributions on the T3A and T3B flat-plate cases. [33]

3.1.2 Case 2: NLF(1)-0416 Airfoil

The second test case is the NLF(1)-0416, natural-laminar-flow airfoil designed by Somers for low-speed general aviation applications [28]. A wind-tunnel test campaign was conducted for this airfoil and covered a wide range of Reynolds numbers; however, only the $Re = 4 \times 10^6$ conditions were chosen for the workshop. The reason for this is that the available dataset also includes measured bounds for the transition locations at this Reynolds number, and the upper-surface transition mechanism is expected to be natural transition in an adverse pressure gradient for much if not all of the low-drag lift-coefficient range (the so-called "drag bucket"). A laminar separation bubble forms upstream of the lower-surface cove; however, experience with this airfoil has shown this bubble to be only minimally interactive. This case is regarded as a 2D validation case because it allows the models to be tested for a realistic aerodynamic shape.

While this case was more forgiving than the flat-plate, there was still significant spread across participants/codes/models. This behavior is visible in the grid convergence results for lift and drag coefficient at $\alpha = 0^\circ$ as shown in Fig. 2 and in the drag polar shown in Fig. 3. Because all participants used different models, it is impossible to isolate, or even narrow down, the exact cause of the scatter.



(a) Lift Coefficient (b) Drag Coefficient

Figure 2 – NLF(1)-0416 force-coefficient grid convergence for $\alpha = 0^\circ$ and $Re = 4 \times 10^6$.[33]

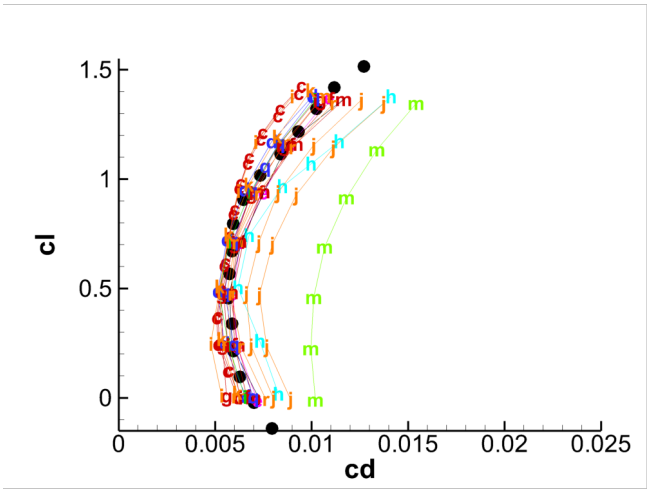


Figure 3 – Predicted NLF(1)-0416 drag polars for $Re = 4 \times 10^6$.[33]

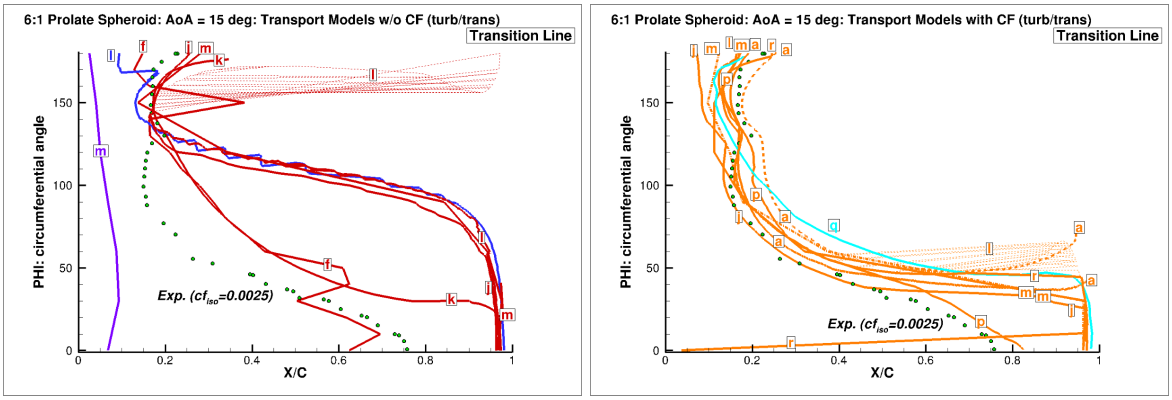
3.1.3 Case 3: 6:1 Prolate Spheroid

The 6:1 prolate spheroid [29] was chosen as a three-dimensional verification and validation case due to its geometric simplicity and relative economy in required mesh size. It is also a configuration that captures some characteristics of flow over a fuselage, and it is often used in the calibration of cross-flow transition models. Nevertheless, being a three-dimensional case presented a marked increase in computational expense over the two-dimensional cases, which slightly reduced the number of participant data submissions despite the geometric simplicity. It was also observed that approximately only one half of the submissions for this case used a model with crossflow transition physics.

For $\alpha = 5^\circ$, the impact of a dedicated crossflow transition model was minimal. As the angle of attack increases to 15°, however, the flow becomes less axisymmetric and the impact of crossflow transition becomes very pronounced. A comparison of models with and without dedicated crossflow modeling for the higher angle is shown in Fig. 4.

3.1.4 Case 4: CRM-NLF

The fourth and final test case was the CRM-NLF. This configuration is a proof-of-concept for the CAT-NLF design philosophy [34, 30]. The model was tested at high Reynolds numbers in the NASA National Transonic Facility (NTF) with temperature sensitive paint to visualize the transition fronts on the wing upper surface. [35] Overall this case garnered more interest from workshop participants than the prolate spheroid, presumably because it was transonic (making it more relevant to practical applications) and because it was based on the Common Research Model (providing a connection to



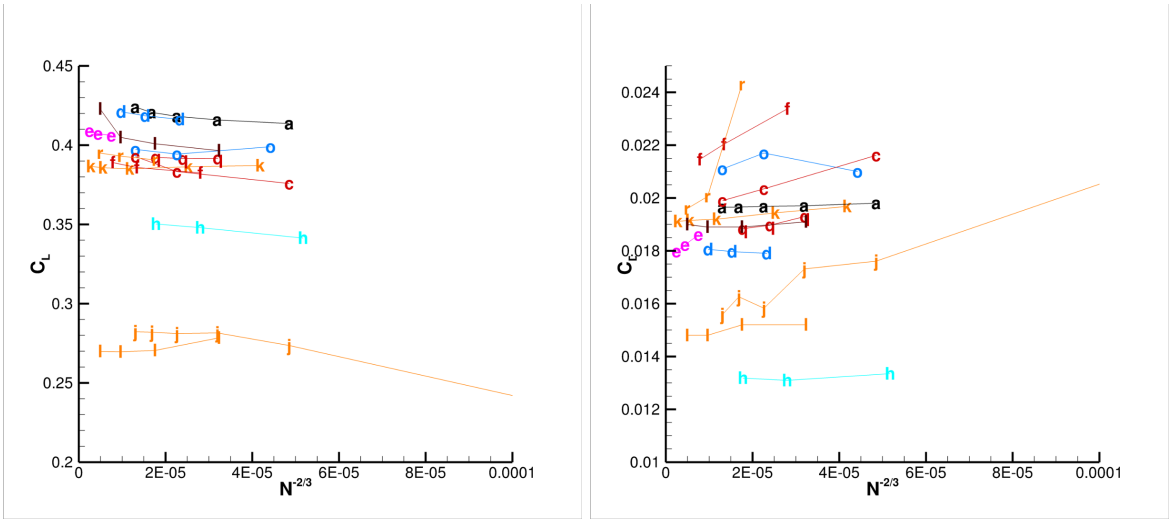
(a) Without Crossflow Modeling

(b) With Crossflow Modeling

Figure 4 – Effect of crossflow transition modeling on the 6:1 prolate spheroid at $\alpha = 15^{\circ}$ and $Re = 6.5 \times 10^{6}$.[33]

other prediction workshops).

Participant data showed significant spread in forces and moments. An example of this is included as Fig. 5 which depicts the $\alpha = 1.98^{\circ}$ grid convergence. A major contributor to the spread was inconsistency across codes/models in predicting the shock location on the wing upper surface. An example of this is shown in Fig. 6. This is much more spread than is typically found in fully turbulent simulations, and seems to result from strong viscous-inviscid interactions due to the shockwave/boundary-layer interactions. Participants who used the Menter-type models largely reported upstream transition locations, but their reported skin-friction distributions suggested a larger spread in transition locations. Further inquiry into this discrepancy revealed fundamental issues with the turbulence index used to evaluate transition location.



(a) Lift Coefficient.

(b) Drag Coefficient.

Figure 5 – CRM-NLF force-coefficient grid convergence for its cruise point.[33]

3.2 Outcomes

The workshop was successful in assessing the current state of the art in predicting laminar-turbulent transition using RANS CFD methods, and participants were willing to take risks and try novel model combinations. While best practices were not identified, there was cross-pollination of ideas across participant teams. Nevertheless, there was still room for improvement in the workshop: it was not successful in providing verification of model implementations, and it remains an open question. Many

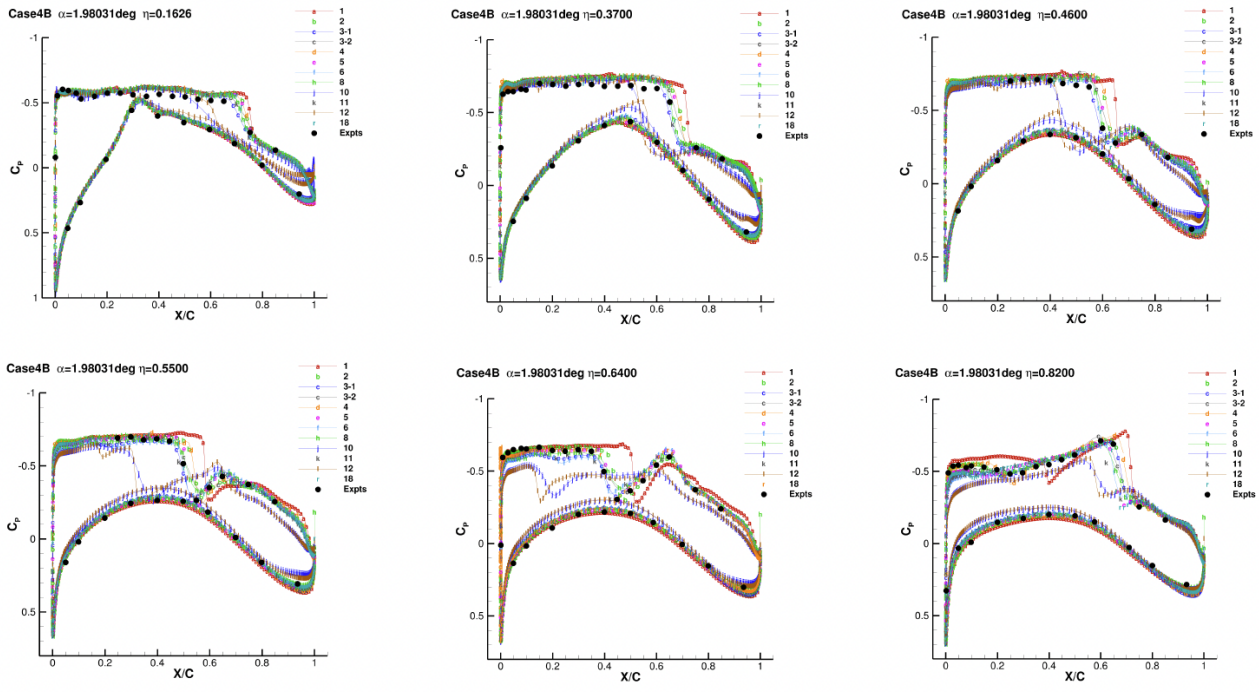


Figure 6 – Predicted pressure distributions at various wing stations of the CRM-NLF at its cruise point.[33]

custom variants of models were used within each major transition modeling framework, and it was noticed that variations in an accompanying turbulence model can have leading-order effects on the transition prediction. This was especially true with the viscous-inviscid interactions of the CRM-NLF case causing strong coupling between the transition point and the mean flow. In the aftermath of the workshop, multiple groups took the initiative to establish verification benchmarks [36, 10] for the Langtry-Menter model due to its prevalence in the community. It was also observed during the workshop that transition location was not a robust verification metric, partly because there were no acceptable turbulence indices at the time. This led to follow-on work by Carnes and Coder [37] who derived a turbulence index for the Langtry-Menter transition/turbulence model and confirmed its behavior.

4. Persisting Modeling Challenges

4.1 Locality and Disparate Transition Mechanisms

One of the most challenging aspects of predicting laminar-turbulent boundary-layer transition using single-point-closure, PDE-based models is that transition is an inherently non-local process. In low-turbulence environments, which are typical for external aerodynamic flows, the path to transition is dominated by linear growth of instabilities as described by wall-normal eigenmodes. There are no global/universal characteristics of the flow to anchor a model. By contrast, turbulence models are able to exploit self-similar behaviors in the inertial regime matched up to a universal law of the wall. Although turbulence may be non-local, its effect on the mean flow can often be well-predicted with local, single-point closure relations.

Under the broad scope of boundary-layer transition, there are multiple potential mechanisms that need to be treated independently. This is true whether the model is PDE-based, or if higher-fidelity, stability-based methods are employed. [2] For example, there are Tollmien-Schlichting waves, separation-induced transition, crossflow instabilities, hypersonic second-mode instabilities, bypass transition, etc. Each of these is driven by different flow physics. Many PDE-based models account for multiple

[2] DNS can capture all of the physics in a single simulation; however, the prediction depends on accurate specification of quantities like free-stream turbulence spectra and surface roughness, which are often unknown.

transition mechanisms to enable broad usage; however, this creates a verification challenge: the set of test cases or the manufactured solutions need to excite all terms in the model. Consider, for instance, the Langtry-Menter model with a crossflow modeling extension. [3, 15]. Different transition scenarios that need to be independently verified (based on required `if-then` statements and `min/max` operators) include

- Natural transition in a favorable pressure gradient
- Natural transition in an adverse pressure gradient
- Separation-induced transition, such as via a laminar separation bubble or shockwave
- Bypass transition in a favorable pressure gradient
- Bypass transition in an adverse pressure gradient
- Crossflow transition

By contrast, the original, as-published version of the Spalart-Allmaras model requires no explicit `if-then` statements and only one `min` function to account for finite-precision arithmetic at an asymptotic limit [32]. Therefore, the work required to verify a PDE-based transition model is generally much greater than for a turbulence model since a substantial portion of the model is passive at any given point in the flow.

4.2 Free-Stream Turbulence Sustainment

A key element of model verification is consistent application of boundary conditions both at the wall and in the free stream. For models based on the Menter $k-\omega$ SST turbulence model [31] (and other two-equation turbulence models), the decay of turbulence quantities in quiescent free-stream flow becomes a concern for external aerodynamic flows. For the SST model, the decay is given by the general forms

$$\omega = \frac{U_\infty}{\beta_2 x + c_1} \tag{1}$$

$$k = c_2 \left(\beta_2 x + c_1\right)^{-\frac{\beta^*}{\beta_2}} \tag{2}$$

where the constants c_1 and c_2 are case-specific.

Available experimental data from the popular T3-series of transitional flat plates include the measured turbulence intensities along the length of the plate outside of the boundary layer. Although fitting c_1 and c_2 is relatively straightforward, evaluating the equations upstream of the plate reveals that k and ω become singular a relatively short distance ahead of the plate. In other words, if the inlet is placed too far upstream of the leading edge, there are no real values of k and ω on the inlet that match the turbulence intensity distribution over the plate. This led to the standard grid family to have an inlet that is closer than expected to the leading edge. Additionally, the decay behavior is the reason for the abnormally large inlet eddy viscosity recommended for the T3B case [3, 8] to arrest the decay.

For airfoil test cases it has been recommended by the author [38] that the far-field boundary be placed at least 1000 chords from the surface to mitigate its influence on integrated drag. As a result, the values of k and ω, as well as ν_t, are very small when the flow reaches the airfoil. The values are so low that Menter transition models use a limited value. This also reduces, if not eliminates, the sensitivity of the flow to changing free-stream turbulence levels.

To overcome this problem for external flows with large, open domains, various methods have been proposed to sustain the turbulence levels. An early attempt was that of Rumsey and Spalart [39, 40] which add production terms that attract the solution to k_∞ and ω_∞. The strength of the attractor is

weak enough that there is little impact on a fully turbulent boundary layer; however, they remain active upstream of transition and contaminate the laminar boundary layer. This has prompted various approaches to suppressing the sustaining terms in the laminar region. The DLR TAU code uses a spatial switch to ensure the sustaining terms are active only outside of the boundary layer and/or upstream of the model [41]. Other methods, such as proposed by Lopes et al. [42], use solution-based switches to preserve the laminar region. In the author's opinion, this is still an open topic and no single method of sustaining free-stream turbulence has emerged as superior.

4.3 Robust Tripping

Another challenge is constructing terms that trip the flow from laminar to turbulent without strong dependency on grid resolution or variations in the turbulence model. For example, the Langtry-Menter model [3] relies on turbulence kinetic energy near the edge of the boundary layer to diffuse inward and seed the transition process. For instance, the choice of the TKE source term has a leading-order effect on the transition location such as depicted in Fig. 7. The primary reason for this is the so-called stagnation-point anomaly. With the strain-based source term, the excess production around the stagnation point provides high values of available TKE around the stagnation point. Conversely, a Kato-Launder source term [43] has less available TKE at both stagnation and transition, and transition is slightly further downstream. The newer Menter γ transition model [4] addresses the tripping problem by introducing an additional production term into the turbulence kinetic energy equation.

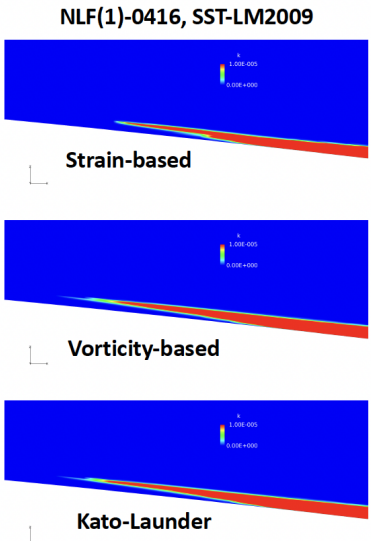


Figure 7 – Contours of Langtry-Menter intermittency variable showing the effect of TKE production term definition on transition behavior on the NLF(1)-0416 upper surface.
(Results courtesy of Dr. Jared Carnes)

The SA-AFT model suffers from an entirely different problem. In the standard formulations of the model (e.g. AFT2014 or AFT2019), the eddy viscosity grows in the laminar boundary-layer at transition via two modeling terms: the source term $c_{b1}\Omega\tilde{\nu}_t$ and the non-linear diffusion term $c_b 2\nabla\nu_t \cdot \nabla\nu_t$. The source term acts based on a residual, background level of ν_t/ν and provides exponential growth. While it may be superficially compelling, it creates an unintended dependency on how close to zero ν_t is (i.e., 10^{-6} and 10^{-9} may both be acceptable approximations to zero), it can provide orders of magnitude difference in how the source term grows turbulence. The non-linear diffusion term was intended for transverse gradients, but the transition front activates the term with sharp streamwise gradients. This term enables the turbulence to push upstream, particularly when there is coarse streamwise grid spacing. Recent developments in the SA-AFT model framework by Gosin et al. [11] have proposed a new trip term that can grow eddy viscosity from a fully laminar initial state. This alternative was used successfully by Simpson et al. [44], though more experience with this variant is required before any conclusions can be drawn.

4.4 Calculation of Pressure-Gradient Parameters and Crossflow Sensors

A third persisting challenge is construction of the solution-based sensors to determine the margin to transition. This includes both pressure-gradient parameters (which are interchangeable with laminar boundary-layer shape factors) and crossflow sensors. The Langtry-Menter model was the first PDE-based model to include dedicated, calibrated effects of pressure gradient on transition. It uses a local parameter

$$\lambda_\theta = \frac{\theta^2}{\nu}\frac{dU}{ds} \tag{3}$$

which is based on the integral Thwaits-Walz parameter with θ estimated based on wall distance. The model is calibrated based on the value of λ_θ at the edge of the boundary layer to calculate the transitional momentum-thickness Reynolds number $\widetilde{Re_{\theta,t}}$, which is then diffused into the boundary layer. While this parameter has been used with success, it is not Galilean invariant and the requirement that it diffuse into the boundary layer creates convergence challenges.

The original version of the AFT model used the local shape factor,

$$H_L = \frac{\Omega d}{U_e} \tag{4}$$

to capture pressure gradient effects. While the numerator is fully local, the denominator is an estimate of the velocity at the edge of the boundary layer. Closure is provided by assuming isentropic flow outside of the boundary layer,

$$\left(\frac{\gamma}{\gamma-1}\right)\frac{P_\infty}{\rho_\infty} + \frac{1}{2}U_\infty^2 = \left(\frac{\gamma}{\gamma-1}\right)\frac{P}{\rho_e} + \frac{1}{2}U_e^2 \tag{5}$$

$$\rho_e = \rho_\infty\left(\frac{P}{P_\infty}\right)^{1/\gamma} \tag{6}$$

This local shape factor was found to be very useful for estimating integral boundary-layer properties, but the isentropic assumption limited its applicability to the subsonic and transonic regimes for steady flows.

Subsequently, Menter introduced a new, fully local pressure gradient parameter defined as

$$\lambda_\theta = \frac{d^2}{\nu}\frac{\partial}{\partial n}(\vec{u}\cdot\hat{n}) \tag{7}$$

The derivative in this expression is the wall-normal derivative of the wall-normal component of velocity as a generalization of $\frac{\partial v}{\partial y}$ in conventional boundary-layer coordinates. This term is fully local and Galilean invariant, which is a compelling quantity. It also prompted the author to adopt it in the AFT2017 [20] and AFT2019 [6] variants aimed primarily at rotorcraft simulations. Although this pressure gradient parameter has been used successfully in some codes, it is prone to numerical issues. Adjoint-based mesh adaptation studies by Gosin showed difficulty grid converging the parameter with noise/irregularity that persisted [11]; however, there may be a sensitivity to the manner in which wall distance is calculated that has not been fully explored [44].

4.5 Differentiability and Numerical Robustness

A pervasive issue with PDE-based transition models is the difficulty of converging them to machine zero and achieving grid-independent solutions. Much of this is anecdotal, though there have been some documented studies such as the ones by Venkatachari et al. [10] and Vogel et al. [45]. A common best practice is that structured/quad surface meshes provide better, more consistent predictions than triangular meshes, but it is commonly expected that the two mesh types will predict different transition fronts for the same geometry.

One of the major hindrances of transition model convergence is the prevalence of limiters and

switches that are non-differentiable. Recognizing this, there have been several attempts at constructing "smooth" variants of the models. Piotrowski and Zingg [46] worked to smooth out all non-differentiable features of the Langtry-Menter model correlations as coupled with the Spalart-Allmaras turbulence model, and they were able to demonstrate significant improvement in residual convergence. Gosin et al. [11] did something similar with the SA-AFT model to implement it in a finite-element solver with adjoint-based mesh adaptation, and Simpson et al. [44] went even further by introducing a pressure gradient parameter with better numerical behavior.

5. Plans for Second AIAA Transition Modeling and Prediction Workshop

Building on the successes and recognizing the lingering open questions from the first workshop, a second workshop (CFDTMPW-2) is planned for AIAA SciTech 2027 (a "pre-workshop") and AIAA Aviation 2027 (the main workshop), with activities already underway. A feature of the second workshop is the adoption of the Technology Focus Group (TFG) model, first used in the High-Lift Prediction Workshop series, for organizing activities. This allows participants to focus on one (or more) focus areas aligned with their individual/organizational priorities without needing to devote temporal and computational resources running cases not of interest. For this workshop, the TFGs are divided based on flight regime, as each presents its own physical and numerical challenges. These are Low-Speed, Transonic, and Hypersonic.

Transcending the TFGs is a concerted effort to verify model implementations. To this end, participants have been encouraged to implement the Langtry-Menter model [3]. Many codes, whether commercial, government, or academic, feature a $\gamma - Re_{\theta,t}$-type transition model coupled with the SST turbulence model, so converting the implemented correlations to the as-published ones is feasible.

5.1 Technology Focus Groups

5.1.1 Low-Speed

The Low-Speed TFG is tasked with studying the predictive capabilities of models in the fully subsonic regime. Arguably, this is the most mature regime since it aligns well with the intended use cases of many existing PDE-based models, and it lacks the complications associated with shockwaves. Four test cases have been identified for the second workshop:

1. NLF(1)-0416 airfoil
2. Infinite swept wing
3. NASA Juncture Flow Model
4. TU Braunschweig SE2A 3d/x-wing

The NLF(1)-0416 airfoil case is the same as from the first workshop, as it has become a standard test case for PDE-based models across the community. The family of structured C-grids provided for the first workshop go to a resolution 2113×289 points, while Venkatachari et al. [10] extended the family to 4225×577 points.

The other three test cases are new for the second workshop and feature varying levels of geometric complexity. All of them have a strong influence from crossflow transition. The infinite swept wing case uses the NACA 64_2A015 airfoil and is based on the experiment of Boltz et al. conducted in the NASA Ames 12-ft wind tunnel [47]. The NASA Juncture Flow Model [48] is a more modern test case for which detailed experimental measurements are available. A further benefit of the Juncture Flow Model is that the geometric definition is fully parametric, which is anticipated to enable higher quality mesh generation and reduced ambiguity in how the model is computationally represented. Finally, the TU Braunschweig SE2A wing is an evolution of the Petzold-Radespiel sickle wing that provides spanwise-varying crossflow [49].

5.1.2 Transonic

The Transonic TFG focuses on test cases relevant to commercial aviation. Two test cases have been selected:

1. VA-2 Supercritical Airfoil
2. CRM-NLF

The CRM-NLF case is the same as in the first prediction workshop, as the participant data spread warrants further study in the second workshop. A downside of this case is that its three-dimensionality makes a full verification study prohibitively expensive for some participants. Therefore, a cheaper alternative was identified in the VA-2 supercritical airfoil [50]. The VA-2 case is based on the work of Costantini [51] and has a Reynolds number of 10×10^6, which will exercise the models' ability to predict natural transition. A grid family for the VA-2 has been generated using conformal mapping methods to ensure smoothness and consistency across all levels and made available to workshop participants. The provided grid resolutions range from 199×49 to 4753×1153 points.

5.1.3 Hypersonic

A flight regime that elicits great community interest is that of hypersonics. Boundary-layer transition at these regimes behaves quite differently than for subsonic and transonic flows, as the thermoacoustic second Mack mode often becomes the dominant streamwise instability. Further complicating hypersonic transition prediction is that the entire flight vehicle (or test article) is influenced by shock-dominated flow. Unlike transonic flows where the outer flow remains isentropic (or nearly so) until the main shock on the wing, hypersonic articles have strong shockwaves at the nose. Thus, the entire boundary-layer flow, including the transition process, sets up downstream of a shockwave. If the leading-edge is blunt, the curved bow shock introduces entropy gradients and an entropy layer that itself influences the transition process. Prior studies by Cutrone et al. [52] highlight the sensitivity of leading models to seemingly arbitrary user choices. Although the same test case cannot be used in the workshop, three cases have been identified:

1. T4 Hypersonic Flat Plate
2. HIFiRE-5 Elliptic Cone
3. HIAD IRVE Scallop-5

These cases span from canonical to complex, allowing the hypersonic transition modeling capabilities to be fully exercised. The flat-plate case is based on the experiments by Mee in the University of Queensland T4 shock tunnel [53]. With the geometric simplicity, this case is also being used for verification studies with 13 levels of grid resolution being provided to participants. The HIFiRE-5 case is the primary three-dimensional test case, striking a balance between three-dimensionality and geometric simplicity (it is parametrically defined). The test conditions are based on the experiments by Juliano et al. in the Purdue BAM6QT [54]. The Hypersonic Inflatable Aerodynamic Decelerator (HIAD) test case is a bluff-body case and represents the importance of boundary-layer transition in atmospheric (re)entry. The conditions are based on those from the NASA LaRC 20-inch, Mach 6 tunnel.

6. Conclusion

Verification and validation of PDE-based transition models remains an open topic. The AIAA CFD Transition Modeling and Discussion Group serves to promote such activities within the relevant technical communities (modelers, practitioners, code developers, etc.), and has organized two AIAA CFD Transition Modeling and Prediction Workshops. The first, CFDTMPW-1, was held in 2021. Unfortunately, verification was impossible due to each participant team using a different model. It also was not always clear which metric should be used to compare results (e.g., skin friction at a given location, integrated force and moment) to definitively quantify the solution. Transition location is not valid for comparison since it is a distributed process, and at the time there was no robust turbulence

index. The second workshop, CFDTMPW-2, is being held in 2027, and has divided the effort into three Technology Focus Groups based on flight regime, each with their own set of test cases. By having separate validation cases, the transition criteria that are most relevant can be assessed.

The author hopes that CFDTMPW-2 will lead to a database of verified solutions against which developers can benchmark their implementation of existing models and/or assess the predictive accuracy of new models. The author also hopes that progress continues toward addressing the persisting challenges of predicting transition in an industrial CFD environment.

7. Contact Author Email Address

Mailto: Dr. James G. Coder jgc5005@psu.edu

8. Copyright Statement

The authors confirm that they, and/or their company or organization, hold copyright on all of the original material included in this paper. The authors also confirm that they have obtained permission, from the copyright holder of any third party material included in this paper, to publish it as part of their paper. The authors confirm that they give permission, or have obtained permission from the copyright holder of this paper, for the publication and distribution of this paper as part of the ICAS proceedings or as individual off-prints from the proceedings.

Acknowledgments

The author is extraordinarily grateful for the contributions of numerous students and collaborators over the past 10+ years to help further the state of the art in industrial transition modeling. Names are not included here for fear of accidentally omitting somebody.

References

[1] D. K. Walters and J. H. Leylek. A new model for boundary-layer transition using a single-point rans approach. *Journal of Turbomachinery*, 126:193–202, Mar. 2004.

[2] D. K. Walters and D. Cokljat. A three-equation eddy-viscosity model for reynolds-averaged navier-stokes simulations of transitional flows. *Journal of Fluids Engineering*, 130:1–13, Dec. 2008.

[3] R. B. Langtry and F. R. Menter. Correlation-based transition modeling for unstructured parallelized computational fluid dynamics codes. *AIAA Journal*, 47(12):2894–2906, December 2009.

[4] Florian R. Menter, Pavel E. Smirnov, Tao Liu, and Ravikanth Avancha. A one-equation local correlation-based transition model. *Flow, Turbulence and Combustion*, 95(4):583–619, December 2015.

[5] J. G. Coder and M. D. Maughmer. Computational fluid dynamics compatible transition modeling using an amplification factor transport equation. *AIAA Journal*, 52(11):2506–2512, November 2014.

[6] J. G. Coder. Further development of the amplification factor transport transition model for aerodynamic flows. In AIAA Paper No. 2019-0039*, Proceedings of the AIAA Scitech 2019 Forum*, San Diego, CA., January 2019.

[7] David W. Levy, Kelly R. Laflin, Edward N. Tinoco, John C. Vassberg, Mori Mani, Ben Rider, Christopher L. Rumsey, Richard A. Wahls, Joseph H. Morrison, Olaf P. Brodersen, Simone Crippa, Dimitri J. Mavriplis, and Mitsuhiro Murayama. Summary of data from the fifth computational fluid dynamics drag prediction workshop. *Journal of Aircraft*, 51, 2014.

[8] J. G. Coder. Standard test cases for transition model verification and validation in computational fluid dynamics. In AIAA Paper No. 2018-0029*, Proceedings of the 2018 AIAA Aerospace Sciences Meeting, AIAA SciTech Forum*, Kissimmee, FL, Jan. 2018.

[9] R. B. Langtry and F. R. Menter. Transition modeling for general CFD applications in aeronautics. In AIAA Paper No. 2005-0522*, 43rd AIAA Aerospace Sciences Meeting and Exhibit*, Reno, NV, Jan. 2005.

[10] Balaji Shankar Venkatachari, Preethi V. Mysore, Nathaniel Hildebrand, Meelan M. Choudhari, and Marie F. Denison. Verification of the $\gamma - re_{\theta,t}$ transition model in overflow and fun3d. *Journal of Aircraft*, 61, 2024.

[11] Samuel A. Gosin, James G. Coder, Marshall C. Galbraith, Steven R. Allmaras, and Nicholas J. Wyman. Assessment of amplification factor transport transition modeling using output-based mesh adaptation. *AIAA Journal*, 64:57–80, 2026.

[12] S. C. Cakmakcioglu, O. Bas, and U. Kaynak. A correlation-based algebraic transition model. *Proceedings of the Institution of Mechanical Engineers, Part C: Journal of Mechanical Engineering Science*, 232:3915–3929, 2018.

[13] J. G. Coder. Evaluation of cfd transition modeling for transonic, natural-laminar-flow design. *34th Congress of the International Council of the Aeronautical Sciences*, ICAS Paper 2024-1179, Florence, Italy, September 2024.

[14] F. R. Menter, A. Matyushenko, R. Lechner, A. Stabnikov, and A. Garbaruk. An algebraic lctm model for laminar–turbulent transition prediction. *Flow, Turbulence and Combustion*, 109(10):841—869, 2022.

[15] R. B. Langtry, K. Sengupta, D. T. Yeh, and A. J. Dorgan. Extending the γ - Re_θ local correlation based transition model for crossflow effects. In AIAA Paper No. 2015-2474*, 22nd AIAA Computational Fluid Dynamics Conference*, Dallas, Tx, June 2015.

[16] C. Grabe and A. Krumbein. Correlation-based transition transport modeling for three-dimensional aerodynamic configurations. *Journal of Aircraft*, 50(5):1533–1539, September-October 2013.

[17] C. Grabe, N. Shengyang, and A. Krumbein. Transport modeling for the prediction of crossflow transition. *AIAA Journal*, 56(8):3167–3178, August 2018.

[18] Z. Liu, Y. Liu, J. Li, and C. Yan. Local correlation-based transition model for high-speed flows. *AIAA Journal*, 60(3):1365–1381, 2022.

[19] M. Drela and M. B. Giles. Viscous-inviscid analysis of transonic and low reynolds number airfoils. *AIAA Journal*, 25(10):1347–1355, October 1987.

[20] J. G. Coder. Enhancement of the amplification factor transport transition modeling framework. In *Proceedings of the AIAA Aerospace Sciences Meeting, AIAA SciTech Forum*, Grapevine, TX, January 2018.

[21] C. J. Axten, J. G. Coder, T. R. Wayman, D. Freund, A. Vogel, and N. Pfeiffer. Cfd transition model calibration for transonic, natural-laminar-flow applications. *AIAA 2026 Aviation Forum*, AIAA Paper 2026–4163, San Diego, CA, June 2026.

[22] J. A. Carnes and J. G. Coder. Effect of crossflow on the S-76 and PSP rotors in hover. In AIAA Paper No. 2020-0773*, Proceedings of the AIAA Scitech 2020 Forum*, Orlando, FL., January 2020.

[23] B. Barraza, A. Gross, M. Leinemann, C. Hader, and H. F. Fasel. Neural network-based hypersonic crossflow transition model. *Journal of Spacecraft and Rockets*, 62(2):372–385, 2025.

[24] P. Ströer, N. Krimmelbein, A. Krumbein, and C. Grabe. Stability-based transition transport modeling for unstructured computational fluid dynamics including convection effects. *AIAA Journal*, 2020.

[25] L. Pascal, G. Delattre, D. Hugues, and J. Cliquet. Stability-based transition model using transport equations. *AIAA Journal*, 58(2):2933–2942, 2020.

[26] Z. Liu, Y. Liu, J. Li, and C. Yan. Fully local transition closure model for hypersonic boundary layers considering crossflow effects. *AIAA Journal*, 59(5):1692–1706, 2021.

[27] P. E. Roach and D. H. Brierley. The influence of a turbulent free-stream on zero pressure gradient transitional boundary layer development. part i: Test cases t3a and t3b. In *ERCOFTAC Workshop*, Cambridge, March 1990. Cambridge University Press.

[28] D. M. Somers. Design and experimental results for a natural-laminar-flow airfoilfor general aviation applications. NASA TP-1981-1861, NASA, 1981.

[29] H. P. Kreplin, H. Vollmers, and H. Meier. Wall shear stress measurements on an inclined prolate spheroid in the dfvlr 3m x 3m low speed wind tunnel. Technical report, Von Karman Institute for Fluid Dynamics, Göttingen, 1985. Tech. Rep. IB-22-84-A-33, DFVLR-AVA.

[30] Michelle N. Lynde and Richard L. Campbell. Computational design and analysis of a transonic natural laminar flow wing for a wind tunnel model. *35th AIAA Applied Aerodynamics Conference*, AIAA Paper 2017–3058, Denver, CO, June 2017.

[31] F. R. Menter. Two-equation eddy viscosity turbulence models for engineering applications. *AIAA Journal*, 32(8):1598–1605, August 1994.

[32] P. R. Spalart and S. R. Allmaras. A one-equation turbulence model for aerodynamic flows. *Recherche Aerospatiale*, pages 5–21, 1994.

[33] J. G. Coder. Summary of the 1st aiaa cfd transition modeling and prediction workshop. NASA Ames Advanced Modeling Simulation Seminar Series, March 2021.

[34] M. N. Lynde and R. L. Campbell. Computational design and analysis of a transonic natural laminar flow wing for a wind tunnel model. In AIAA Paper No. 2017-3058*, Proceedings of the 35th AIAA Applied Aerodynamics Conference, AIAA AVIATION Forum*, Denver, CO, June 2017.

[35] M. N. Lynde, R. Campbell, M. B. Rivers, S. A. Viken, D. T. Chan, A. N. Watkins, and S. L. Goodliff. Preliminary results from an experimental assessment of a natural laminar flow design method. In AIAA Paper No. 2019-2298*, Proceedings of the AIAA Scitech 2019 Forum*, San Diego, CA, January 2019.

[36] J. A. Carnes and J. G. Coder. Benchmarking the langtry-menter transition model using overflow for the aiaa transition modeling workshop. *AIAA 2022 Aviation Forum*, AIAA Paper 2022–3680, Chicago, IL, June-July 2022.

[37] J. A. Carnes and J. G. Coder. Analyzing the near-wall behavior of the langtry–menter transition model. *Flow, Turbulence and Combustion*, 108(5):683–715, 2022.

[38] J. G. Coder and M. D. Maughmer. Numerical validation of the squire-young formula for profile-drag prediction. *Journal of Aircraft*, 52:948–955, 2015.

[39] Philippe R. Spalart and Christopher L. Rumsey. Effective inflow conditions for turbulence models in aerodynamic calculations. *AIAA Journal*, 45(10):2544—-2553, 2007.

[40] Christopher L. Rumsey and Philippe R. Spalart. Turbulence model behavior in low reynolds number regions of aerodynamic flowfields. In *38th AIAA Fluid Dynamics Conference and Exhibit*, Seattle, WA, June 2008. AIAA Paper 2008-4403.

[41] A. Krumbein, D. G. Francois, and N. Krimmelbein. Transport-based transition prediction for the common research model natural laminar flow configuration. *Journal of Aircraft*, 59(6):1562—1573, 2022.

[42] Rui Lopes, Luis Eça, Guilherme Vaz, and Maarten Kerkvliet. A technique to control the decay of freestream turbulence for transitional flow simulations. *AIAA Journal*, 60(6):3565—3580, 2022.

[43] M. Kato and B. E. Launder. The modeling of turbulent flow around stationary and vibrating square cylinders. *Proc. 9th Symposium on Turbulent Shear Flows*, pages 10.4.1–10.4.6, August 1993.

[44] Anna Simpson, Marshall C. Galbraith, and Steven R. Allmaras. A numerically tolerant formulation of the amplification factor transport transition model. *AIAA Journal*, Articles in Advance, 2026.

[45] Ethan A. Vogel, Meelan Choudhari, and Balaji S. Venkatachari. Assessment and grid convergence study of rans-based transition models for high-speed flows. *Journal of Spacecraft and Rockets*, 62:1676–1697, 2025.

[46] M. G. H. Piotrowski and D. W. Zingg. Smooth local correlation-based transition model for the spalart–allmaras turbulence model. *AIAA Journal*, 59(2):474–492, February 2021.

[47] F. W. Boltz, G. C. Kenyon, and C. Q. Allen. Effects of sweep angle on the boundary-layer stability characteristics of an untapered wing at low speeds. *NASA TN D-338*, 1960.

[48] Andrew Leidy, Michael A. Kegerise, Judith Hannon, Meelan M. Choudhari, Balaji Shankar Venkatachari, and Pedro Paredes. Measurements and computations of natural transition on the nasa juncture-flow model with a symmetric wing. *AIAA 2023 SciTech Forum*, AIAA Paper 2023–0441, National Harbor, MD, January 2023.

[49] R. Petzold and R. Radespiel. Transition on a wing with spanwise varying crossflow and linear stability analysis. *AIAA Journal*, 53(2):321–335, 2015.

[50] P. Thiede and E. Stanewsky. Active and passive shock/boundary layer interaction control on supercritical airfoils. *Techn. Report AGARD CP-365*, 1984.

[51] M. Costantini, T. Lee, T. Nonomura, K. Asai, and C. Klein. Feasibility of skin-friction field measurements in a transonic wind tunnel using a global luminescent oil film. *Experiments in Fluids*, 62(21):1–34, 2021.

[52] Luigi Cutrone, Antonio Schettino, José I. Cardesa, Grégory Delattre, Steven Qiang James G. Coder, Ethan Vogel, and Meelan Choudhari. Predicting hypersonic boundary-layer transition on complex geometries with rans models. *CEAS Space Journal*, 2025.

[53] D. J. Mee. Boundary-layer transition measurements in hypervelocity flows in a shock tunnel. *AIAA Journal*, 40(8):1542–1548, 2002.

[54] T. J. Juliano, L. A. Paquin, and M. P. Borg. Hifire-5 boundary-layer transition measured in a mach-6 quiet tunnel with infrared thermography. *AIAA Journal*, 57(5):2001–2010, 2019.